Version 2.2
November 7, 2018

Precision Time-of-Flight at the Fermilab Testbeam Facility

William Badgett, Dmitri Denisov, Petra Merkel, Sergei Nagaitsev, Adam Para, Erik Ramberg, Luciano Ristori
Fermi National Accelerator Laboratory
B. W. Adams, C. Ertley, M. Foley, A. Lyashenko, M. J. Minot, M. Popecki, W. Worstell
Incom, Inc; Charlton, MA 01507
H. J. Frisch, B. W. Adams (Incom, EFI-UC), E. Angelico, M. Bogdan, A. Elagin, C. Grosso-Pilcher, M. Heintz, R. Jiang, R. Northrop, C. Pilcher, E. Spieglan; M. Caliskan (undergraduate)
Enrico Fermi Institute, University of Chicago

Abstract

The first commercially-produced LAPPD^{TM} photodetectors are now available from Incom, Inc [1]. We propose to follow up the measurements with 2" Planacon MCP-PMTs in T979 [2, 3, 4] and T1075 [5] to optimize the timing resolution and to characterize the performance and life-time of two of the newly available 8" Incom modules at the Fermilab Testbeam Facility . The tests would use the 10 Gsample/sec PSEC4 waveform sampling electronics system developed by Eric Oberla et al. If successful we would then propose an upgrade of the Fermilab Testbeam Facility Time of Flight(TOF) system to up to 4 LAPPDs for particle ID. The goals thus are two-fold: 1) an installed long-term upgrade to the Fermilab Test Beam Facility; and 2) a validation of a new commercially-available technology for future detectors at the Energy and Luminosity Frontiers.

Contents

1 Introduction

In 2006 Ohshima [6] demonstrated 5 psec resolution for charged particles traversing a radiator on the face of an Micro-Channel Plate Photomultiplier (MCP-PMT) [7]. Subsequently T979 demonstrated resolutions down to 7.7 psec in MTEST [4]. More recent studies at the Argonne APS using a fast laser [8] extrapolate the current LAPPD^{TM} Signal/Noise ratio down to 1-2 psec resolution for large signals, possibly limited by the laser spot size.

Since then Incom, Inc has started to produce the first commercially available $8'' \times 8''$ LAPPD^{TM} MCP-PMTs, Chicago has further developed the 10 GHz PSEC4 waveform sampling readout system [9, 10], and the Optical TPC concept has been demonstrated at Fermilab [5]. We propose to instrument the Test Beam Facility with a LAPPD^{TM} Time-of-Flight (TOF) system with the goals of taking a step toward broader familiarity with the technology in the particle physics community, exploration of the achievable TOF resolution in a working setting, and the improvement of particle identification for users at the FTBF.

1.1 Factors That Determine the Achievable Timing Resolution with MCP-PMTs

The LAPPD Collaboration was formed in 2009 to do the necessary R&D to build large-area psec-resolution detectors for charged particle identification at the Fermilab Tevatron Collider and Large Hadron Collider at CERN [11]. At the first of the workshops on determining the limits in fast timing [12] there was spirited debate on the most promising techniques and the factors that limit the resolution. Subsequent development of electronics and photodetectors, and detailed measurements [13] have pushed the uncertain region down to ≈ 5 psec [14]. Figure 1 illustrates the current understanding of the criteria necessary to achieve time resolutions well below ≈ 10 psec [15].

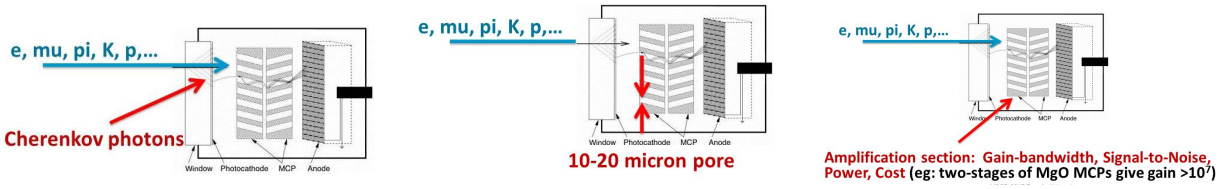

Figure 1: Illustrations of the three necessary detection criteria for psec-level timing: 1) A fast source of light with many photo-electrons so that the average arrival rate is on the order of 1 per psec; 2) A small amplification pixel size compared to the distance light travels in 1 psec, 300 microns, to limit the time spread; and 3) high gain such that a single photo-electron determines the measured time.

1.2 The Ritt Parameterization of Resolution versus Bandwidth and Noise

Figure 2 shows a table from Stefan Ritt's talk at the Second Chicago Photocathode Workshop characterizing the predicted timing resolution using waveform sampling [16]. For a fixed number of digitized samples on the leading edge of the pulse the dependences on Signal/Noise ($U/\Delta U$) and bandwidth are predicted to be linear. Current $LAPPD^{\rm TM}$ values are shown in the last row [17]. This is of course an extrapolation by more than an order of magnitude[1] However LAPPD data follow the rule-of-thumb down to 6 psec and extrapolate to 1-2 psec, as shown in Figure 3 [8]. It is this extrapolation we want to test.

1.3 Goals: 1. Addition of Permanent Wide-band Particle ID to MTest, and 2. Establishment of Cherenkov MCP-PMTs as a Robust Workhorse Technology

The primary goal is addition of a permanent wide-band particle identification system to the MTEST beamline, as described below in Section 5.

It is a truism that a new detector technology, with capabilities well beyond previous ones, has to prove itself far from its doting parents. The FTBF offers the unique opportunity to expose a wide international community to routine precision TOF operation and data.

[1] We note that of the relevant parameters, only the bandwidth falls short of the values in the last row of the table. Surface-mount electronics should ameliorate this.

Signal	Noise	Sampling	Bandwidth	Resolution
U	Δu	f_s	f_{3db}	Δt
100 mV	1 mV	2 GSPS	300 MHz	~10 ps
1 V	1 mV	2 GSPS	300 MHz	1 ps
100 mV	1 mV	20 GSPS	3 GHz	0.7 ps
1V	1 mV	10 GSPS	3 GHz	0.1 ps
LAPPD: 1V	0.7 mv	15 GS/sec	1.5 GHz	??

Figure 2: A table from Stefan Ritt's talk at the Second Chicago Photocathode Workshop characterizing the predicted timing resolution using waveform sampling, For a fixed number of samples on the leading edge of the pulse the dependence on the Signal-to-Noise ratio ($U/\Delta U$) and bandwidth is linear. The current measured $LAPPD^{\text{TM}}$ values are shown in the last row.

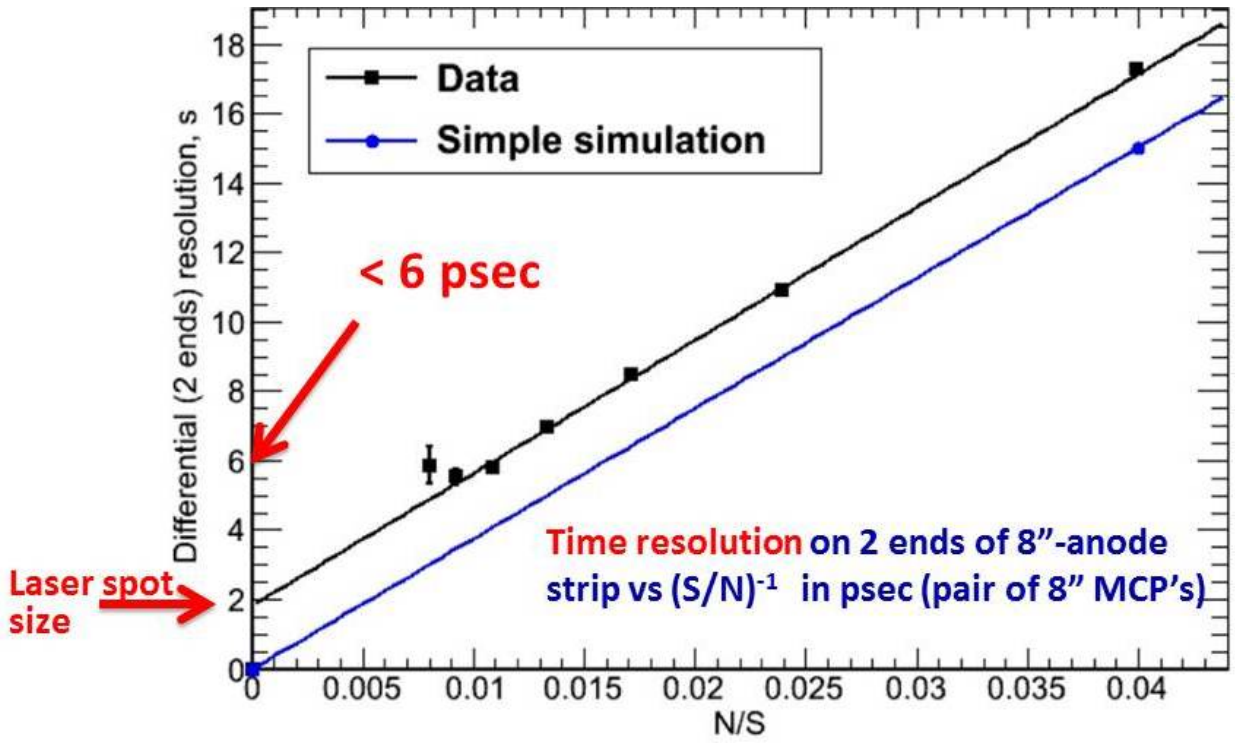

Figure 3: A comparison of the measured time resolution [8] versus the inverse of the Signal/Noise ratio with a simple simulation.

1.4 The Role of the Test Beam in Optimization

A precise determination of the time resolution for charged particles is essential for the consideration of the technology for in future collider detectors. Resolution can be measured well 'on the bench' with a Ti-Saph laser. However there are unique benefits of using a high-energy beam of electrons, muons, mesons, and baryons to complement bench testing:

1. The resolution at the psec level will depend on the time and space spreads of the source photons, the wavelength spectrum, the incident angle of the particle, and secondary interactions/radiation in the detector, all of which are very different from a laser pulse;
2. The test beam is an environment much more like an HEP experiment than a laser lab in terms of cleanliness, access, RF and 60-Hz noise, grounding, cable runs, and breadth of clientele.
3. Installation as an integral part of a user facility tests ease of use, robustness, and long-term maintainability.

1.5 Applications

The most appealing application for psec or sub-psec resolution for charged particles is vertexing and flavor/family flow identification at future colliders in particle and heavy-ion colliders [18]. This is an area in which a proximity-focused Cherenkov-radiation based MCP-PMT system has significantly better time resolution than competing large-area technologies (e.g. SiPMTs) for identifying and vertexing charged particles, and vertexing photons. The upgrade to the FTBF would be the first step toward the necessary knowledge for a credible collider system proposal.

In the shorter term, the applications at Fermilab would include a proposed collaboration with the Accelerator Division at IOTA [19] and the ongoing work with LAPPDs in the ANNIE experiment [20].

2 The Incom Generation-I LAPPD

Figure 4 shows a LAPPD^{TM} Gen-I module [17]. The Gen-I modules currently produced by Incom use 50-ohm RF strip lines for good spatial and temporal resolution [21]. The anode strip readout can be straight-forwardly interfaced to the UC PSEC4 digitization and DAQ, which then can be read out using a variety of standard interfaces [9].

2.1 LAPPD^{TM} Mechanical and Performance Specifications

The goals for the mechanical and operational design parameters for the pre-production LAPPD modules are shown in Figures 5 and 6. The current modules do not simultaneously meet all the design parameter goals, but often exceed them individually. This should settle down as preproduction continues, with early modules with character', in Incom's phrase, replaced by modules with less variation if needed [2].

[2]Incom's warranty includes the ability to 'swap' the early modules for later ones as pre-production asymptotically approaches production.

2.2 LAPPD^{TM} Availability

The Incom LAPPD^{TM}s available on the market now are pre-production modules 'with character' i.e. some specs that are not met, typically either peak Quantum Efficiency(QE) or the QE uniformity. These modules will be replaced by Incom with ones with less variation produced later in the pre-production process if needed.

2.3 Generation II and Other Improvements

In addition to the pre-production modules, there are several improvements in the pipeline for which there may be testing opportunities in the FTBF without interfering with the primary goals. Incom and Chicago are collaborating on a 'Generation-II' tile with a ceramic housing and internal capacitively-coupled anode (Fig. 7). The physical dimensions are the same as those of Gen-I, and if these tiles become available we would propose characterization using the same PSEC4 electronics [22] and mechanical mounting. Another possible improvement is use of the PSEC4A chip [23], which has multiple buffers and deadtimeless operation up to 100 KHz. A third initiative is the ongoing development at Incom of MCPs with 10-micron and smaller pores. Going to a smaller MCP pore should reduce the jitter of the 'first strike', which we believe dominates the transit-time spread, and thus significantly improve the time resolution [24].

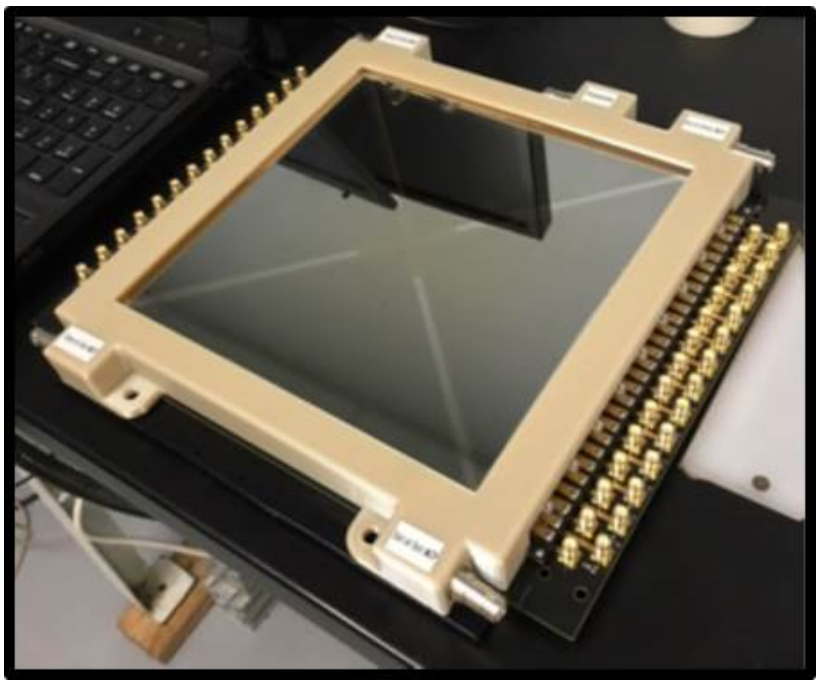

Figure 4: A commercially available Incom LAPPD^{TM} Gen-I module [17].

LAPPD #31 Features, Ratings & Performance

LAPPD #31 General Features and Parameters:

Feature	Parameter
Photodetector Material	Borosilicate Glass
Window Material	Fused Silica Glass
Photocathode Material	Multi-Alkali (K_2NaSb)
Spectral Response (nm)	160-650
Wavelength – Maximum Sensitivity (nm)	≤ 365 nm
Photodetector Active Area Dimensions	195mm X 195mm
• Minimum Effective Area	34,989 mm^2 **[(195*195)- {(2*265*6) – (6x6)}]**
• Active fraction with Edge Frame X-Spacers	92% **[(195*195)- {(2*265*6) – (6x6)}] / (195 * 195)**
Anode Data Strip Configuration	28 silver strips, Width = 5.2 mm, gap 1.7 mm, nominal 50 Ω Impedance
Voltage Distribution	5 taps for independent control of voltage to the photocathode and entry and exit of MCP

LAPPD # 31 Operational Ratings

Parameter	Rating
Supply voltage Photocathode — Anode (Volts)	Typical: • 30V between MCP and photocathode • 900-925 V/mcp • 200 V between MCPs • 200 V between MCP and anode • Photocathode voltage is -2230 to -2255 V Maximum: Photocathode voltage at -2900 V
Operating ambient temperature °C	TBD (nominal room temperature)
Storage temperature °C	-12 to 50 (Avoid indium seal melt)

LAPPD Package / Housing Characteristics

Parameter	Rating
Photodetector Physical Dimensions (L X W X Thickness, mm)	230 x 220 x 22
Photodetector Mounting Case	ULTEM or equivalent dielectric polymer
Photodetector Mounting Case Dimensions	243 mm X 274 mm X 25.2 mm
Connectivity	Passive PC Interface Board , (300 mm X 264 mm X 1.6mm)
Overall Footprint, with Mounting Case & PC Interface Board	300 mm X 274 mm X 26.8 mm
Shipping Container	Pelican Case + Cardboard Box + G-force indicators

Figure 5: The mechanical parameters for Incom Tile 31, one of the recent pre-production LAPPD modules.

LAPPD #31 Features, Ratings & Performance

LAPPD #31 Microchannel Plate (MCP) Features & Performance

MCPs	Two Arranged in a Chevron Pair
Dimensions	203 mm x 203 mm X 1.2 mm
MCP Substrate	Incom C14 Glass
Capillary Pore Diameter (µm) Center to Center Pitch (µm)	20 25
Channel Length / diameter aspect ratio Substrate Thickness (mm)	60:1 1.2
Bias Angle, degrees	13
Capillary Open Area Ratio Percent	68.4
Resistive and Emissive Coatings	Chem 1, Applied via Atomic Layer Deposition (ALD)
Secondary Emission (SEE) Layer Material	MgO
Electrode Penetration – Input & Output (Pore Diameter)	1
MCP ID (Entry / Exit)	C00113-052 / C00113-041
MCP Chevron Pair Gain (@ Measurement & Test)	6.6E6 at 950 V/MCP

LAPPD #31 Operating Performance

Parameter	Performance
MCP resistance in the LAPPD (Entry/Exit)	9.7 / 10.5 Mohms at 900 V E
MCP Dark Rate in the LAPPD (Obtained by setting the photocathode more positive than the entry MCP)	• 0.037 kHz/cm^2 at a threshold of 8E5 gain (134 fC), 925 V/MCP, 30 V positive on photocathode • 0.00015 kHz/cm^2 at a threshold of 8E5 gain (134 fC), 900 V/MCP, 30 V on photocathode [D]
Max Voltage	• 950/950 V/MCP (entry/exit), -2330 volts at the photocathode, or • 900/900 V/MCP (entry/exit), -2400 volts at the photocathode.
Photocathode QE @ 365 nm, max / mean %	14 / 9.8
Photocathode QE Spatial Variability (σ)	1.1%
LAPPD Dark Count rate	• 0.44 kHz/cm^2 at a threshold of 8E5 gain (134 fC), 925 V/MCP, 30 V on photocathode • 0.014 kHz/cm^2 at a threshold of 8E5 gain (134 fC), 900 V/MCP, 30 V on photocathode[D]

Figure 6: The quoted measured operational parameters for Incom Tile 31, one of the recent Incom pre-production LAPPD modules. The measured gain is 8.0×10^6 at 925/925 V (entry/exit MCPs), 30 V on the photocathode, with a variation 50% of the mean.

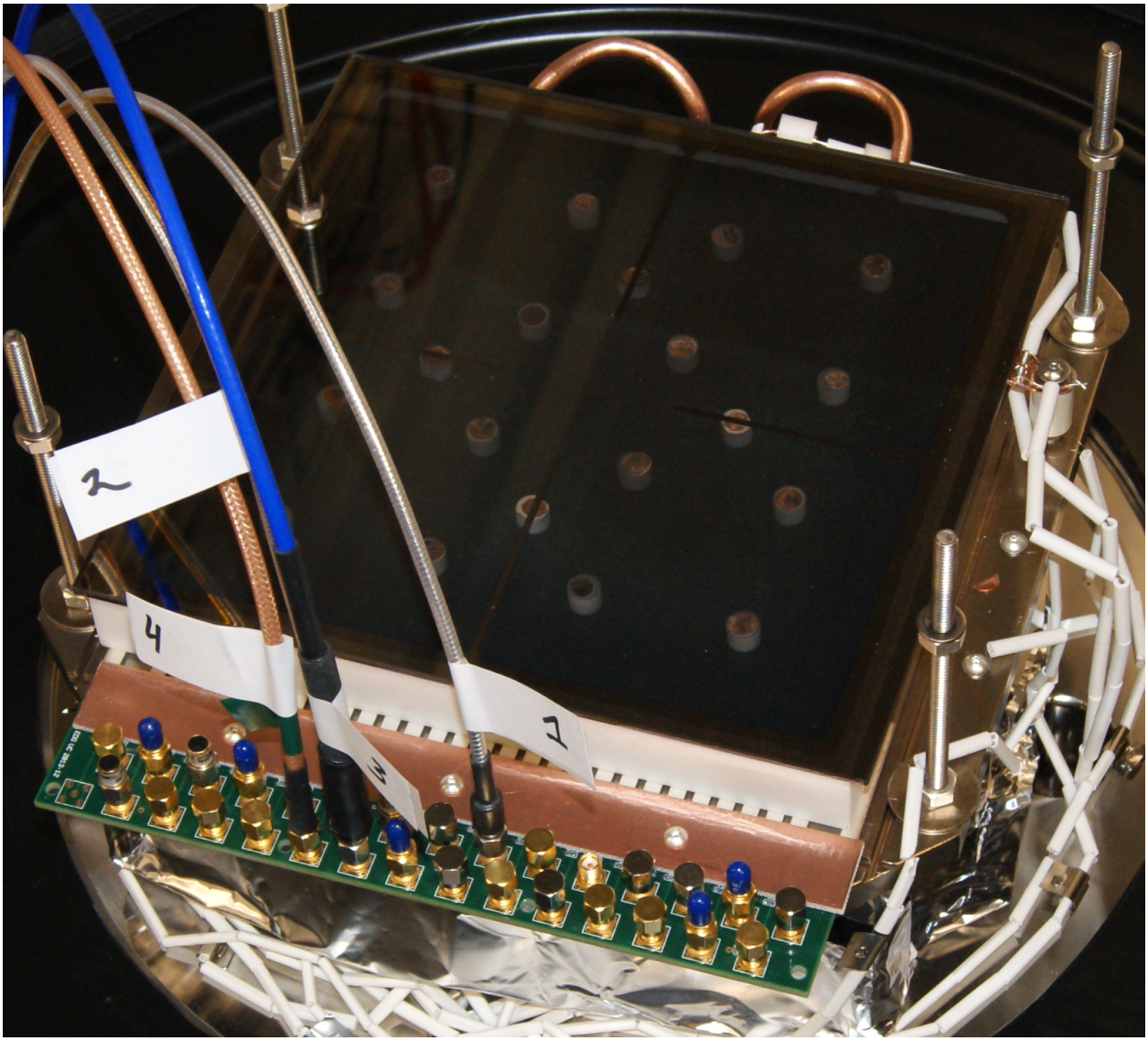

Figure 7: A Prototype UC Generation-II Ceramic LAPPD with capacitively-coupled readout.

3 Compact TOF Detector Station Configurations– Large Pixel Count with Correlated Time and Space Measurement

The correlated time and space resolutions of the LAPPD^{TM} enable several configurations that produce useful time-of-flight and trajectory information. A system of four detectors organized in two separated subsystems, each with two stations spaced by 5-10 meters along the beamline, would provide TOF information over a wide range of momenta. a single subsystem is still useful for characterization of spatial and TOF resolution. Below we briefly describe several geometries.

3.1 Cherenkov Radiator at Entrance Window

Figure 8 illustrates a key principle on which pico-second timing for charged particles is based. This is the simplest geometry, initially proposed and used in T979 [4, 7], and used by Ohshima for his demonstration of 5 psec resolution [6]. In T979 we coupled an 8-mm thick quartz radiator to the front window of a Photonis Planacon [25], generating $\approx$ 50 photo-electrons per charged particle. The advantage is minimum space occupied along the beamline and easy removal from the beam. However one does not get a TOF measurement from a single station. Four such stations, organized into two subsystems, would provide the configuration for the permanent TOF installation in the FTFB, with the ability to remotely withdraw the detectors from the beam for experiments that require a minimum of material in the beam.

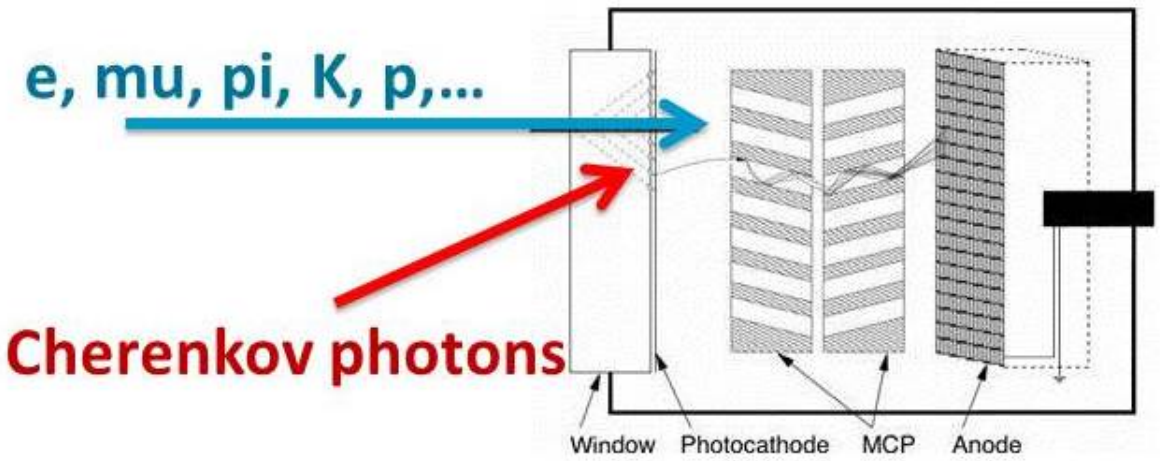

Figure 8: The LAPPD configuration for charged particle MCP-PMT fast timing, with the particle making Cherenkov light in the entrance window and quartz radiator.

3.2 The Optical Time Projection Chamber(Oberla)

The time resolution of LAPPDs is such that one can reconstruct tracks using measurements of the 'drift time' of photons, much as one uses the drift time of electrons in a conventional Nygren Time Projection Chamber(TPC). The technique was demonstrated in the MCenter testbeam (T1075) by Oberla in his Ph.D thesis. Data were taken in a 40-cm long sensitive volume filled with water and observed by Planacon 2" MCP-PMTs, augmented by mirrors that doubled the effective photocathode area and provided transverse spatial information by relative timing [5], as shown in Figure 9. The advantage is one gets spatial track reconstruction in addition to TOF information, even with a single LAPPD^{TM} , suitably augmented by mirrors (more LAPPD coverage is of course better, especially for complex signatures.).

Figure 10 shows the OTPC installed in the MCenter location downstream of the secondary target, where it was exposed to muons. Figure 11 shows the measured times versus position for a muon traversing the OTPC; both the direct and reflected lights form a line, with the position and angle determined by the time difference between the two reconstructed tracks.

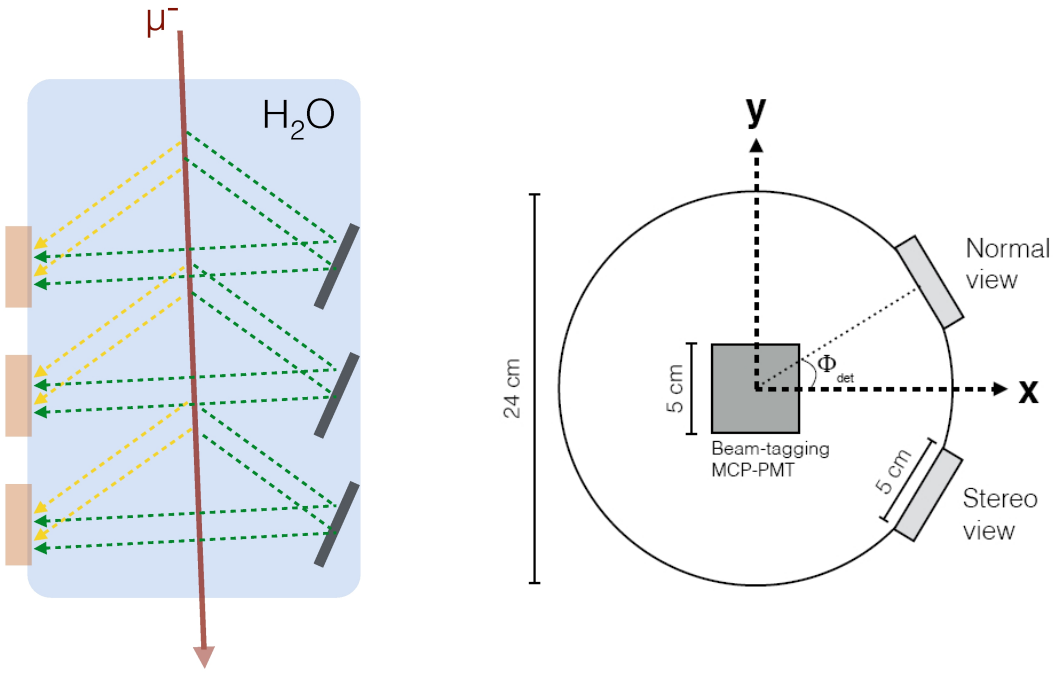

Figure 9: The Optical Time Projection Chamber (OTPC), with Cherenkov light made by charged particles in a long liquid radiator detected by many (90 in this case) measurements with MCP-PMTs along the sides of the container. Mirrors on the opposite side of the volume provide measurements delayed by $\approx$ 790 psec from the direct photons. An elevation view of Eric Oberla's design of the Optical TPC prototype is shown in the left-hand panel. Note the different lengths of the optical paths of the direct and reflected Cherenkov photons. The right-hand panel shows a 'beams-eye' view.

3.3 The MIRCAT Detector (Angelico)

To measure Time-of-Flight at the required precision requires at least two LAPPDs separated by a flight path. However, to get started at the FTBF with the single tube currently being ordered without waiting for a second unit, we have invented a jury-rigged solution, dubbed the MIRCAT, that will allow the commissioning and initial LAPPD characterization using a single module and on-axis particles. Figure 12 shows a schema of the detector, which enables a TOF measurement with a single LAPPD^{TM} module by using two separated radiators in a single housing. The downstream radiator is optically coupled to the window of the LAPPD, as in the T979 geometry. The upstream radiator exploits the same principle as a DIRC [26] to transport the Cherenkov photons by total internal reflection to the edge of the radiator surface. The photons emerging from the slanted edge of the radiator are then reflected (and possibly focused) downstream onto the LAPPD. A simple analysis of the time resolution for this stop-gap 'one hand clapping' geometry is presented in Appendix C; it looks adequate for commissioning. Once more LAPPDs are acquired the MIRCAT will be replaced with a higher-resolution conventional TOF geometry covering the entire beam profile using stations with a larger separation, and Cherenkov light produced only at the face of each photodetector.

A simulation of the optical photons at the LAPPD from a single 8 GeV muon traversing the MIRCAT on the central axis is shown in Figure 13. For clarity, only a small fraction

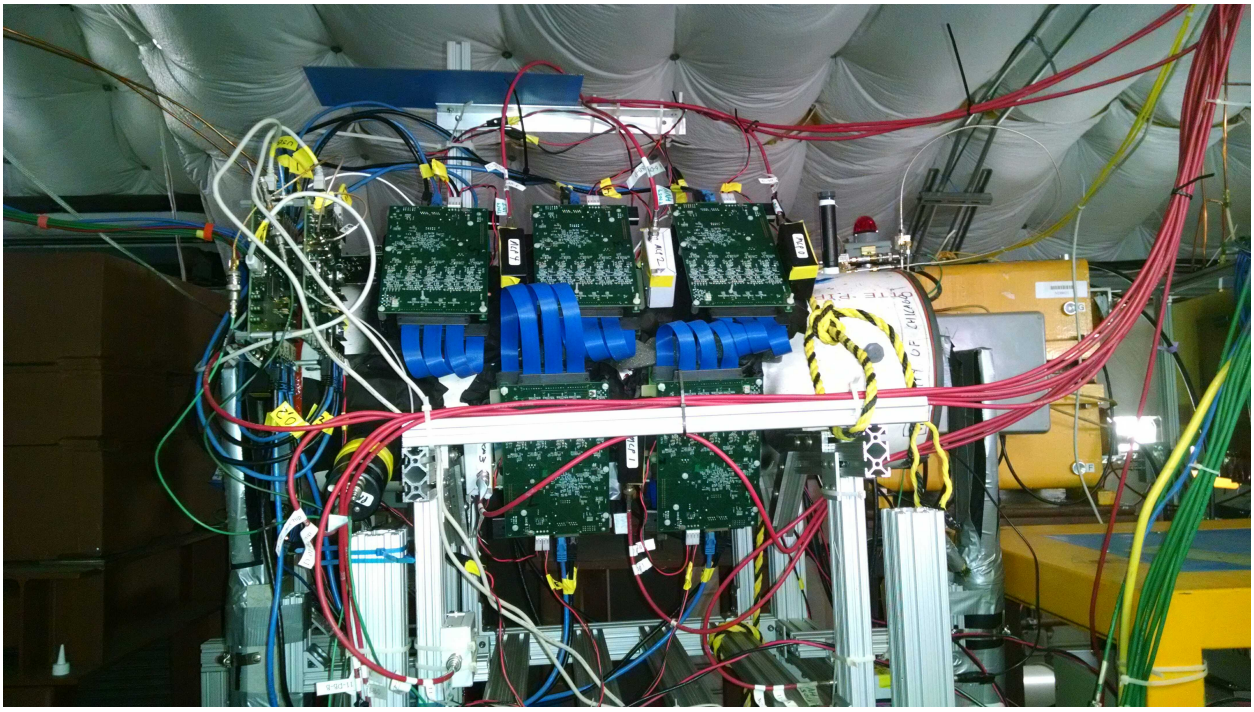

Figure 10: The OTPC installed in the MCenter beamline, with the PSEC4 waveform sampling system and DAQ installed.

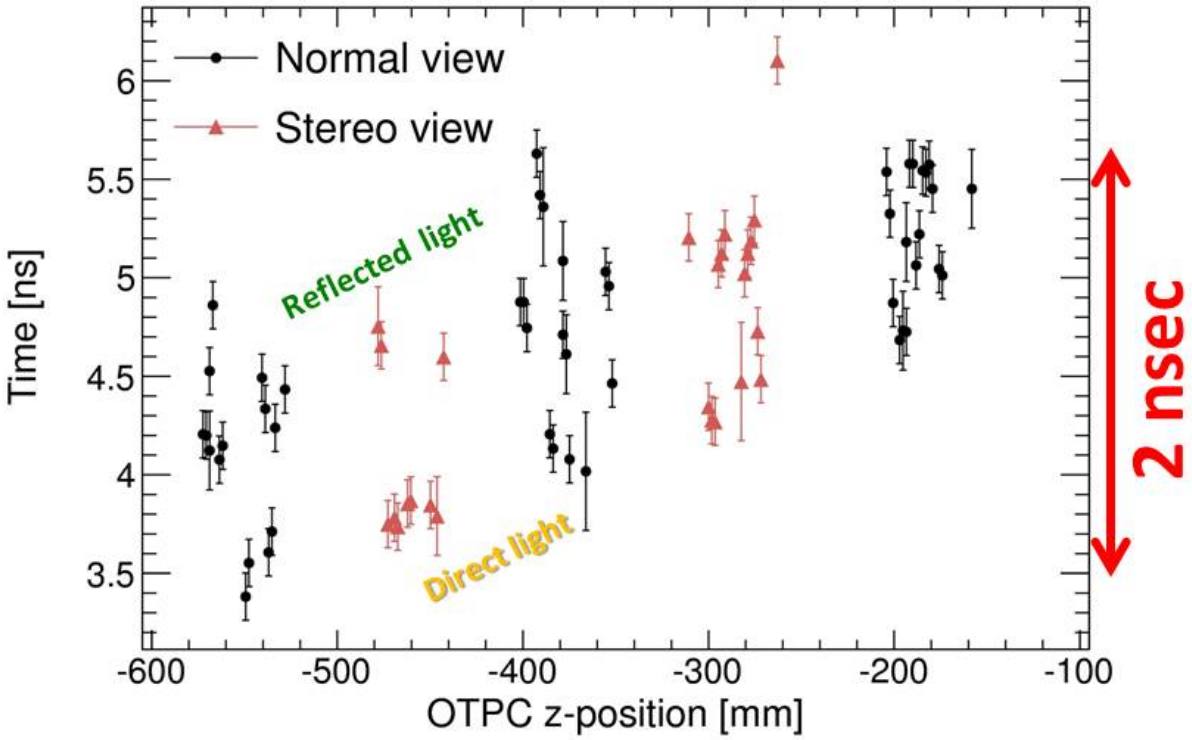

Figure 11: Reconstruction of a single beam particle event in the OTPC; the measured time of arrival of light versus distance along the beam. The earlier light, which forms the lower track, is direct; the reflected light, which constitutes the upper track, arrives 800 psec later.

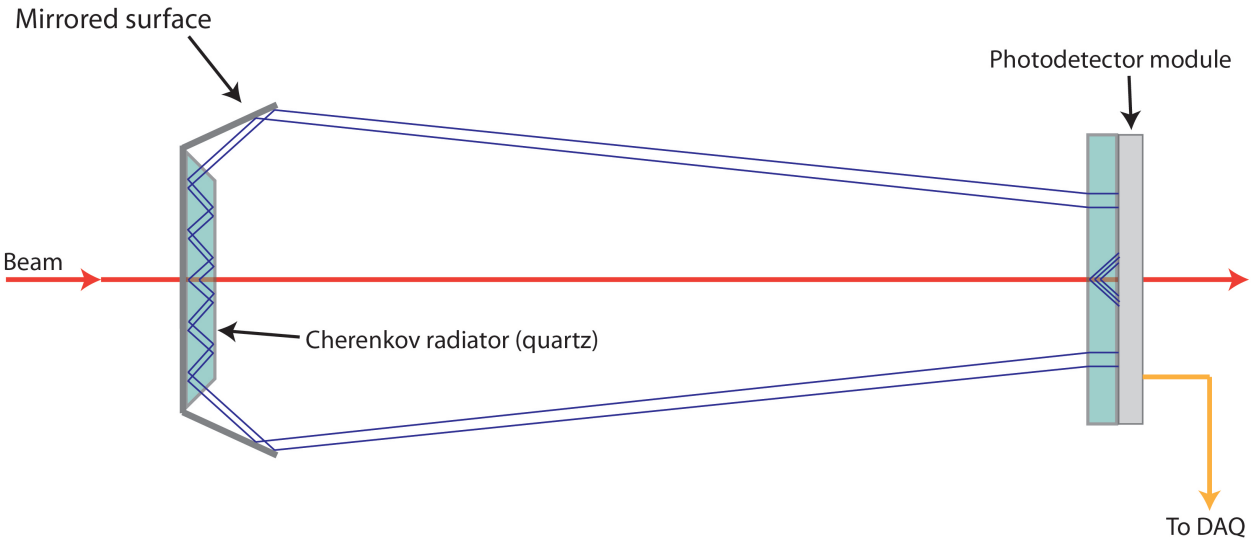

Figure 12: A schema for a 'MIRCAT' TOF detector, which allows a TOF measurement using only a single LAPPD^{TM} module by using two separated radiators in a silvered tube (E. Angelico).

of the photons is shown.

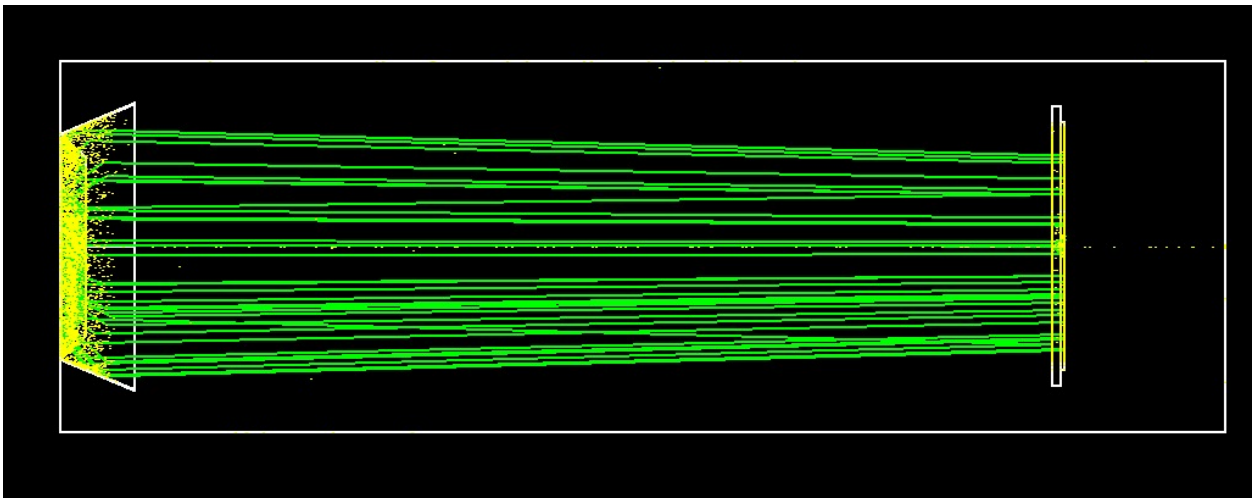

Figure 13: Photons produced by a single on-axis 8 GeV muon in a MIRCAT Geant4 simulation. Only a small fraction of the total light produced is shown.

.

A histogram of the time-of-arrival of optical photons at the LAPPD from 300 muons traversing the MIRCAT on the central axis is shown in Figure 14. The earlier of the two peaks (left-most) is from Cherenkov photons created in the radiator at the LAPPD window. The second peak corresponds to Cherenkov photons from the upstream radiator, which, after emerging from the edge of the quartz, are reflected from the mirrored cylindrical internal surface of the tube onto the LAPPD. The simulation includes dispersion, scattering, and delta-rays.

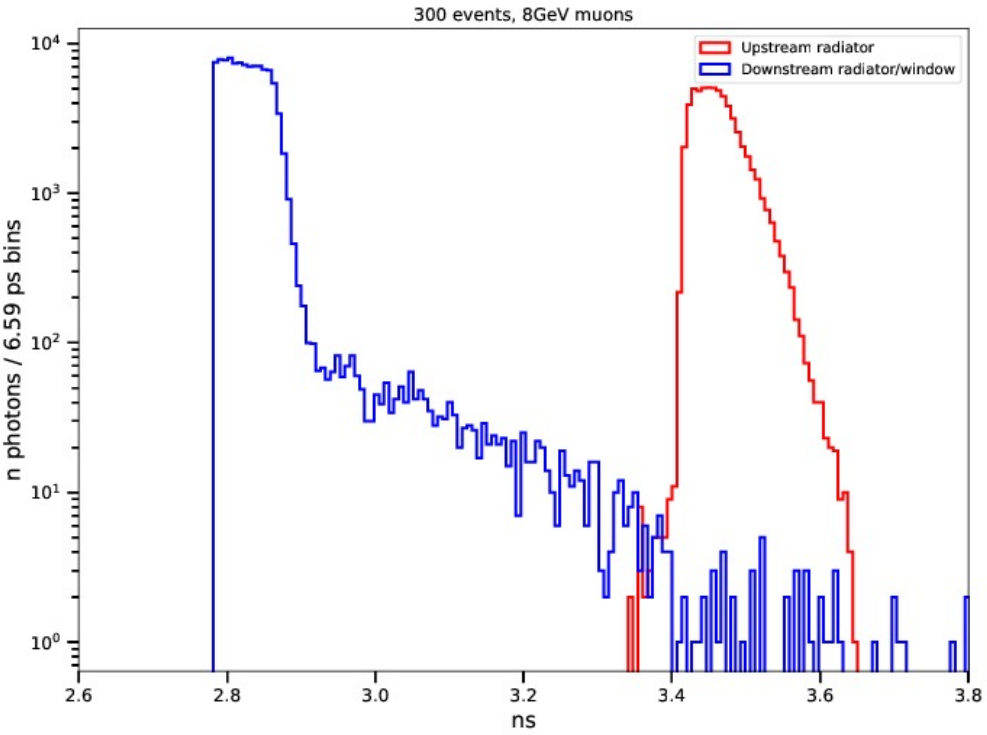

Figure 14: The simulated arrival times of Cherenkov photons at the LAPPD photocathode for 300 on-axis 8-GeV muons in the MIRCAT configuration shown in Figure 12. The earlier peak is from photons from the radiator at the LAPPD window; the second, later, peak is from photons from the upstream radiator.

4 Use of Particle Identification at the Test Beam Facility

Many of the detector-development measurements made at the FTBF are sensitive to the particle type. For example, as calorimetry in collider detectors gets ever-more precise, particle-type-dependent calibration becomes essential. To precisely characterize the resolution for jets of higher-resolution calorimeter designs for future collider detectors in simulations, one needs the capability to measure identified pions, kaons, and protons over the range characteristic of jet fragmentation in very high energy collisions (30-40 GeV at least). Particular effects that are usually integrated over in the simulation response functions, but which will contribute systematic errors to the tails of resolution functions, include:

- differences in π/K interaction lengths;
- differences in π/baryon/anti-baryon interaction lengths;
- differences in K^-/K^+ interaction lengths;
- differences in π^-/π^+ charge-exchange cross-sections;

These can be measured routinely with a fast TOF system.

4.1 Current Installed TOF Particle Identification Capability

Routine particle identification in MTest is currently done with two differential Cherenkov counters and a time-of-flight system. Figure 15 shows the sequence of detectors traversed by the beam [27].

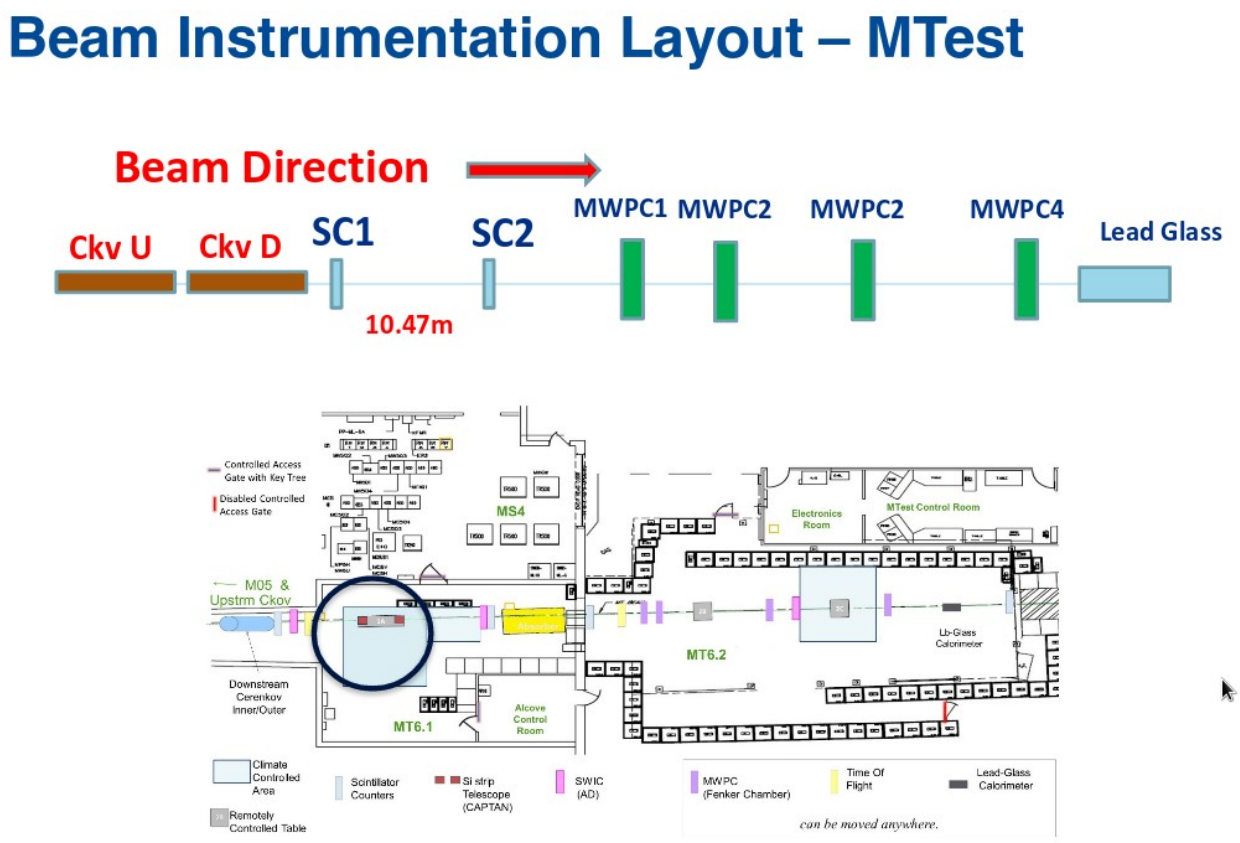

Figure 15: The MTest beam instrumentation layout, showing the sequence of Cherenkov counters, scintillators, MWPCs, and a lead-glass counter (from M. Rominsky, Hadron Production Workshop, July 2017 [27]).

Figure 16 shows the nominal particle composition versus beam momentum for positive particles in the left-hand panel, and for negative particles in the right-hand panel [27].

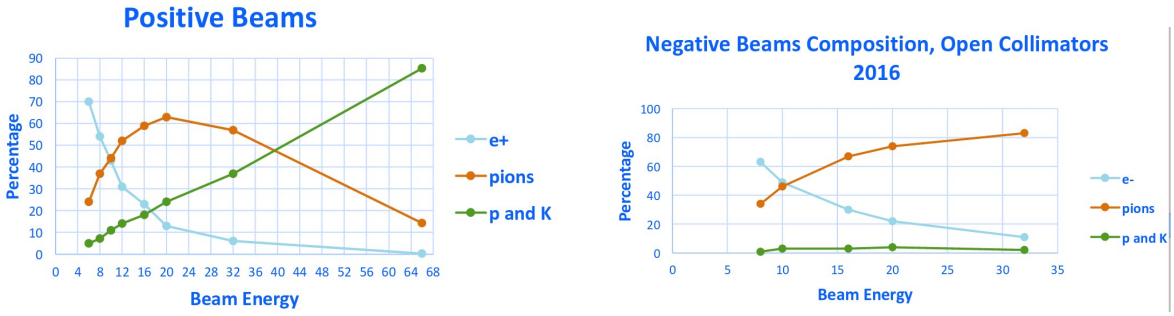

Figure 16: The MTest particle composition versus momentum for positive beam (left) and negative beam (right), as determined by E. Skup and D. Jensen using the Cherenkov counters (from M. Rominsky, Hadron Production Workshop, July 2017 [27]).

4.1.1 Current TOF Hardware and Physical Parameters

The current TOF system was installed in 2014-5 as part of the 'second MINERvA testbeam effort', and is thoroughly described in a detailed note [28]. It consists of two scintillator stations separated by 83.78m (!). The Start station is located in MT3-4; Stop is in MT6.1 (see Figure 15) Each station consists of a single octagon of scintillator, viewed by four photomultipliers on four orthogonal edges. The Start station is 10 cm across; the corresponding dimension for the Stop station is 17.3 cm, with a 'used area' of 12.8cm square [29]. The amount of material in the beam from Start and Stop is 1.24% and 3.0% of a radiation length, respectively. The quoted efficiencies are high: 99% for Start and 97% for Stop. Because the Start station is located in an ODH [3] location, raw signals are brought out on long (82.4m) RG-58 cables with an attenuation factor (voltage) of ≈2.6 to electronics in MT6.1. Typical time jitter is quoted as 300 psec/tube. The overall TOF resolution is quoted as "on the order of 200ps minimum", with caveats on distribution tails and dependence on beam parameters such as momentum bite that affect the path over the 84 meter drift.

4.1.2 Current TOF Particle ID Capability

Protons can currently be separated from lighter particles using the Minerva Test Beam II TOF System up to about 8 GeV at 3σ separation [28].

5 Proposed Extension of Particle ID Capability

. The development of very fast TOF for charged particles, where very fast means resolutions along the particle flight path of less than a few millimeters, is very attractive for future solenoidal and LHCb-geometry detectors at future colliders. It also would allow direct reconstruction of π^0s and ηs from photon arrival times and locations, of importance to elimination of combinatorial backgrounds in high sensitivity in rare decays of kaons and taus. In addition, the unique large footprint of the LAPPD^{TM} detectors covers the footprint of the entire usable beam.

Figures 17, 18 and 19 show the TOF difference between pions and kaons, kaons and protons, and electrons and pions, respectively, versus momentum as a function of separation along the flight path.

5.1 Performance Goals

The TOF performance of the final system in MTESTwill largely be determined by the achievable and maintainable TOF resolution of a single LAPPD station and electronics. and also by system issues related to inter-station timing, dependence on beam trajectories, and mechanical stability over flight paths, as discussed below.

5.1.1 Single Station Time Resolution

The goals for the time resolution of a single station, defined relative to the time of arrival at the photocathode of the charged particle, are set by extrapolations from prior measurements. The goals are extrapolations, and thus include wishful thinking, but the scale and

[3] Oxygen Deficiency Hazard

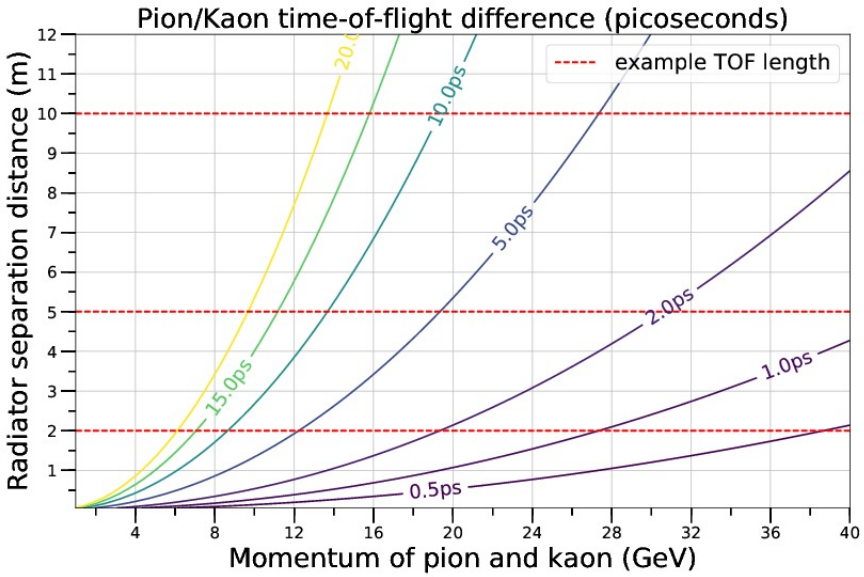

Figure 17: The contours of TOF difference between pions and kaons plotted versus particle momentum (abscissa) and the TOF detector separation (ordinate) (Angelico).

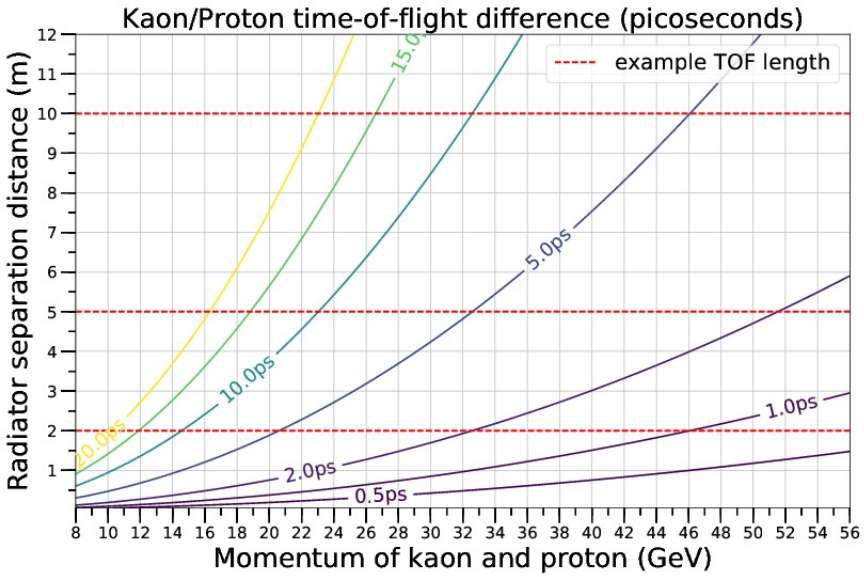

Figure 18: The contours of TOF difference between kaons and protons plotted versus particle momentum (abscissa) and the TOF detector separation (ordinate) (Angelico).

the determining parameters we believe to be largely understood. However it may take time and iterations to achieve the goals.

The input data are the 5 psec resolution measured with charged particles by the Ohshima and the Nagoya group [6], the measurements in the 10 psec range and below of the Fermilab T979 group and collaborators in MTEST [2, 3, 4], and the bench measurements extrapolating to 1-2 psec for large signals by the LAPPD group at the Argonne APS [8]. The wishful thinking is based on the assumptions in the above extrapolation (more below), the reduced first-strike jitter due to the larger bias angle of the Incom MCPs, better attention to noise-reduction in the anode/front-end electronics system, and more sophisticated pulse-

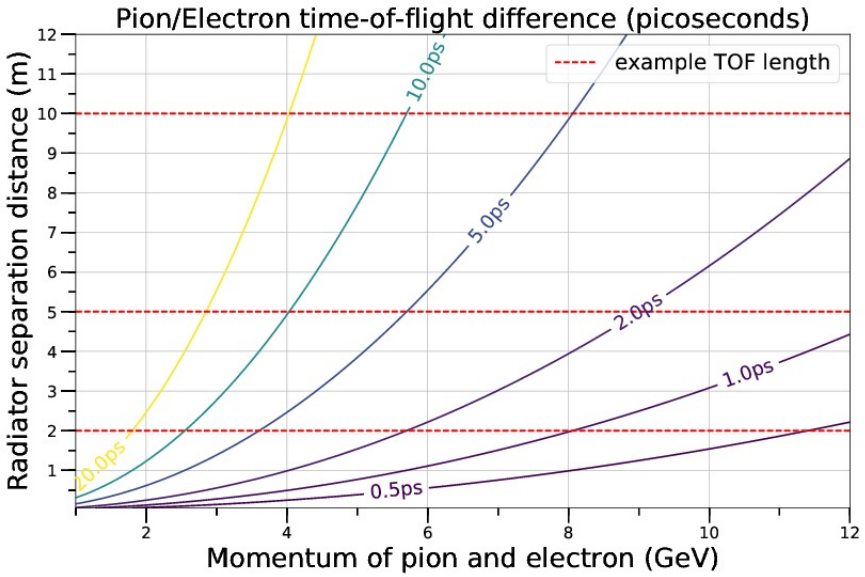

Figure 19: The contours of TOF difference between electrons and pions plotted versus particle momentum (abscissa) and the TOF detector separation (ordinate) (Angelico).

shape timing analysis. However, we will take twice the Ohshima number, 10 psec, as the goal for the one-station resolution of the first implementation. This is consistent with, but more conservative than, the 7.7 psec measured in MTEST by Ronzhin et al. [4].

5.1.2 Two-Station Module Time Resolution

Unlike Cherenkov counters, a TOF system is not set to specific values to discriminate specific velocities, but instead will give velocity data on every particle that is recorded. At most momentum settings of the beam, some mix of electrons, muons, pions, kaons and protons will provide a continuous in-situ calibration. Particle velocities will be calculated relative to peaks in contemporaneous data, sorted by position, trajectory, and time.

Resolutions of a few psec and below constitutes unexplored territory for charged particle time-of-flight. Factors that we will measure and work to minimize in the TOF resolution from 2 stations separated by a drift distance include:

1. Inter-station clock jitter (clock distribution). Jitter cleaners are available at precisions much better than 1 psec [30]. Inter-station calibration over longer periods is intrinsic from electron, muon, pion, kaon, and proton peaks, as applicable, in the data at all momenta (this is an advantage over Cherenkov counters which need to be tuned for beam conditions [31]).
2. Path length variation. LAPPD^{TM} modules provide simultaneous measurement of time and position. With RF stripline readout a resolution of 700 microns in each transverse direction was measured [8]; with a pad readout the resolution was measured to be 300 microns in each direction as long as there was sharing between neighboring pads [32]. Multiple measurements using 4 LAPPDs will provide redundancy.
3. Mechanical/thermal stability. We plan on thermal monitoring as part of the installation. Mechanical stability hopefully will be designed in, including attention to access for alignment and measurement.

4. Path length variations due to scattering. Multiple measurements using 4 LAPPDs will provide redundancy.
5. Accidentals/multiple-tracks/interactions. Multiple measurements using 4 LAPPDs will provide redundancy. We note that the beam in MTest retains the 53 MHz (18.9 nsec bunch separation), and there "rarely are 2 particles/bucket" [29].

5.1.3 Baseline TOF System Time Resolution

Based on the Ohshima measured single-unit 5 psec resolution [6] with MCP-PMTs having lower gain, and hence worse resolution, than LAPPDs, we have set an initial goal of 10 psec differential system resolution. The testbeam would allow tests of later improved LAPPDs with smaller pores or enhanced gain and bandwidth, for example.

5.1.4 Triggering

Unlike the current TOF system which has cables carrying the analog signals to discriminators in crates, the LAPPDs would be digitized at the detectors using PSEC4 waveform sampling. The PSEC4 chips would be operated in self-trigger mode [10], in which the ring buffer is stopped on a signal in a channel. Each 2-detector station would have two scintillator counters, one at each end, to generate a trigger signal for readout and/or reset of that station; trigger logic would allow requiring both stations or not.

It may be possible to use the signals from the PSEC4 chips to make a station signal, to be readout and/or reset by the beam scintillators.

We would like to move to PSEC4A [23] if possible, as the new chip has multiple buffers enabling a longer latency and making the triggering much easier.

5.1.5 Rate Capability

The present TOF system has two stations of areas 10^4 mm^2 and 30 10^4 mm^2, respectively. The Incom LAPPDs have been tested with a laser at rates up to 25 KHz/mm^2 at a gain of 4×10^6. Scaling the current drawn to a gain of 10^7 gives a limit of 10KHz/mm^2. This limit should be largely due to the local nature of the amplification mechanism; scaling to the larger areas of the testbeam profiles should not be a problem, as current is distributed over metalization on the faces of the MCPs. We conclude that there will not be a rate problem for normal operation.

5.1.6 Lifetime

Lead-glass based MCP-PMTs showed a characteristic decrease in gain and photocathode efficiency with extracted charge, severely compromising their attractiveness for use in HEP applications. The Incom LAPPD$^{\text{TM}}$s instead have MCPs that are made of a hard (borosilicate) glass coated by Atomic Layer Deposition (ALD) [33], reducing the ion feedback that damages the photocathode. Recent studies [34] have shown no signs of aging for integrated anode charge up 16C/cm^2. This corresponds to an integrated flux of approximately 4×10^{12} particles per cm^2 for an LAPPD operating at a gain of 10^7. With the typical 4-sec spill once a minute, even with 120 GeV proton beam of several $\times 10^6$/spill [35] one is a long way from radiation damage.

6 Installation and Commissioning Plan

The plan depends on the schedule for acquiring commercial LAPPDs. We consequently have developed phases, starting with a custom station able to measure TOF with only a single LAPPD (Phase I). The goal of Phase II is to build and commission a two-LAPPD subsystem that measures TOF over a path length of 5-8m. Phase III consists of the installation of a second Phase II subsystem. The combined Phase III system provides a redundant check on the particle identification, removing possible low-level ambiguities due to accidentals, scattering and interactions [4]. It also provides the redundancy required for operational robustness. More details are given below.

6.1 Phase I: Design, Installation, and Initial Commissioning of the First LAPPD module

The goals of Phase I are to install and commission an LAPPD detector unit, LAPPD-I, with associated electronics. This unit would be the basis of the units for Phases II and III.

The MIRCAT design allows making precision TOF measurements with a single detector, as the distance between the 2 radiators is known precisely, and the time-sliced optical pattern that arrives downstream on the LAPPD gives both position and angle of the particle trajectory.

As the MIRCAT presents a fair amount of material, we propose running parasitically using muons by setting up downstream of the beam stop shielding in MTest. From T979 we are familiar with the location, operational aspects, cable plant, and counting room.

This phase should give us initial information on the time and space resolutions for a single Incom LAPPD for charged particles. These numbers will be input for the optimization of the next phases, described below. Most importantly, it will allow us to interface to the MTest infrastructures.

6.2 Phase II: Design, Installation, and Initial Commissioning of a 2-LAPPD TOF station.

The goals of Phase II are to install an integrated TOF subsystem consisting of 2 LAPPD stations separated by a drift of 5-8m in MTEST. We are considering locations in MT5 and MT6. Appendix B gives a map of the beam elements [36]. The LAPPD modules themselves occupy 7.5 cm or less along the beamline, but the footprint should be such that we can remotely lower them completely out of the beam for low-momentum electron running.

We note that the digitization and triggering are done locally on the modules, lessening the need for long analog signal cables. We have also developed remote computer control of Droege HV modules so the HV supplies could possibly also be local [37].

Figure 20 shows the concept for Phase II, a single TOF subsystem,incorporating 2 LAPPD detectors.

[4]For example, the current MINERVA TOF system has an RF-structure induced ambiguity at low values of momentum [28].

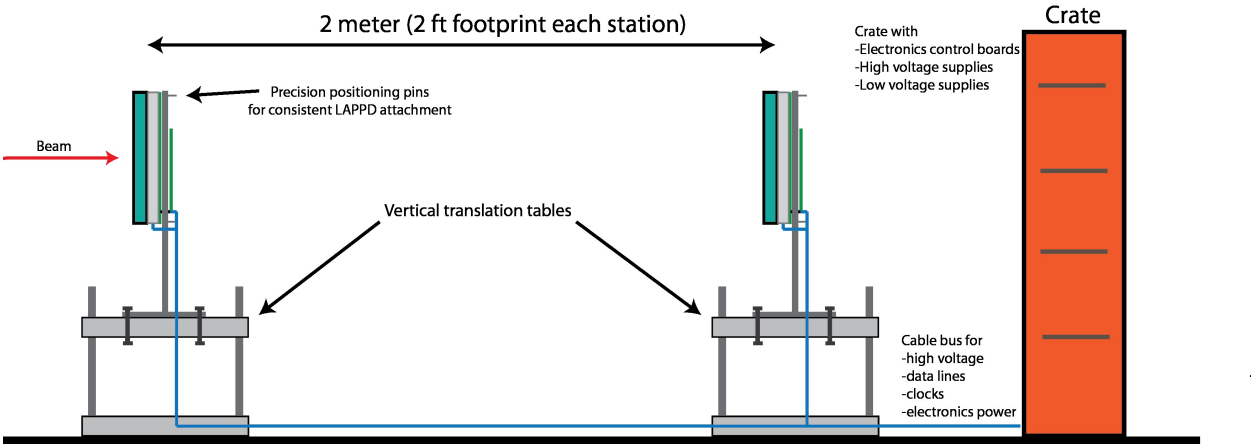

Figure 20: For Phase II, a subsystem of two LAPPD stations will be built and placed at about 2m separation on vertical translation tables for ease of removal from the beam. Electronics will be synchronized and both LAPPDs will operate in self triggering mode.

6.3 Phase III: Implementation of the Long-Term Fermilab Testbeam Facility Psec TOF Configuration

The full MTESTsystem will consist of two TOF subsystems, one upstream and one downstream. Each subsystem would consist of two LAPPD stations, separated by a drift of 5-8m. The combined system provides the high degree of redundancy and robustness necessary for a dependable capability of the FTFB. Figure 21 shows the concept. We note that we are not proposing Phase III here, as the detailed design will be determined by the performance of the Phase II 2-LAPPD subsystem.

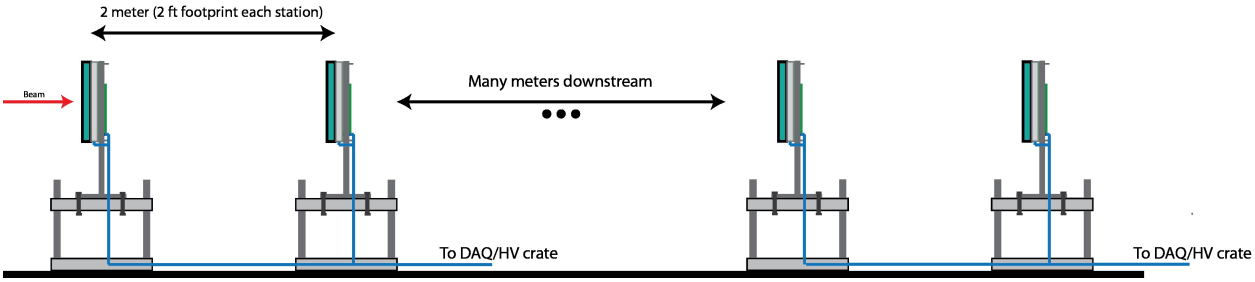

Figure 21: For Phase III, an additional LAPPD subsystem of two LAPPD stations will be constructed using the same hardware as in Phase II.

7 LAPPD Acquisition and Schedule

This will be the third experiment in the test beam for MCP-PMT-based TOF development, following T979 and T1075, but the first with large-area commercial modules with ALD-functionalized hard-glass MCPs. We will be using the same PSEC4 electronics front-end and control system as T1075, with similar DAQ [5].

[5] T1075 used five 30-channel Planacon MCP-PMTs in the OTPC and one to trigger, comparable in PSEC4 system complexity to the four in this proposal.

7.1 LAPPD Acquisition

Incom has several LAPPD modules available for immediate purchase; Fermilab and Chicago have formal quotes in hand. We will need two modules in FY2019, and two in FY2020. Building on the long-time collaboration of Incom with Chicago and Fermilab in LAPPD development, Incom physicists from their LAPPD R&D team will play an active role in the commissioning and detector characterization.

7.2 Schedule

We will need 3 months after delivery of the first LAPPD to build Phase I. With the exception of a relatively simple interface card, we have the PSEC4 waveform sampling electronics in hand for 2 modules. We estimate installation in the T1075 parasitic location in MCenter should take less than a month.

Phase II can begin 2 months after purchase of the 2nd LAPPD, depending on availability of installation time. The schedule for Phase III is obviously contingent on the successful performance of Phase II.

8 Laboratory Resources

Based on our experiences with T979 and T1075, we request the following resources specific to the fast timing:

1. For Phase I, access to the alcove downstream of the cement blocks that form the final shielding for MTest;
2. For Phase II, access to 6-8 feet of beamline in MT6.1 or 6.2.
3. A modest PREP list: a NIM bin, several discriminators and logic units for scintillator trigger counters;
4. Several fast photomultipliers from Anatoly's store;
5. One Droege HV unit per LAPPD (1 for Phase I, 2 for Phase II);
6. Two vertical lift tables for Phase II;
7. HV and signal cables; patch panels;
8. Rack space for 2 crates in the counting room;
9. Safety training, computer accounts, and necessary guidance on Laboratory policies for the Incom personnel.

9 Acknowledgments

We thank JJ Schmidt for invaluable guidance, Leo Bellantoni for a close reading of an early draft and sharing his large store of knowledge, and John Kyle for locational data on the MTest beamline. This effort owes a very large debt to Anatoly Ronzhin, who played a very big role in all aspects of the development of MCP-based psec timing, LAPPD detector development, and in the specific application to TOF capability in the FTBF. We miss him.

Appendix A: Time-of-flight plots for the Minerva 84m separation

The current TOF system installed in MTEST [28] has 2 stations, START and STOP, separated by 84 meters. The plots below have axes extended to cover this range. Note that the current system separates protons from pions up to 8 GeV, which can allow reading off one instance of the effective time resolution from Figure 23 below.

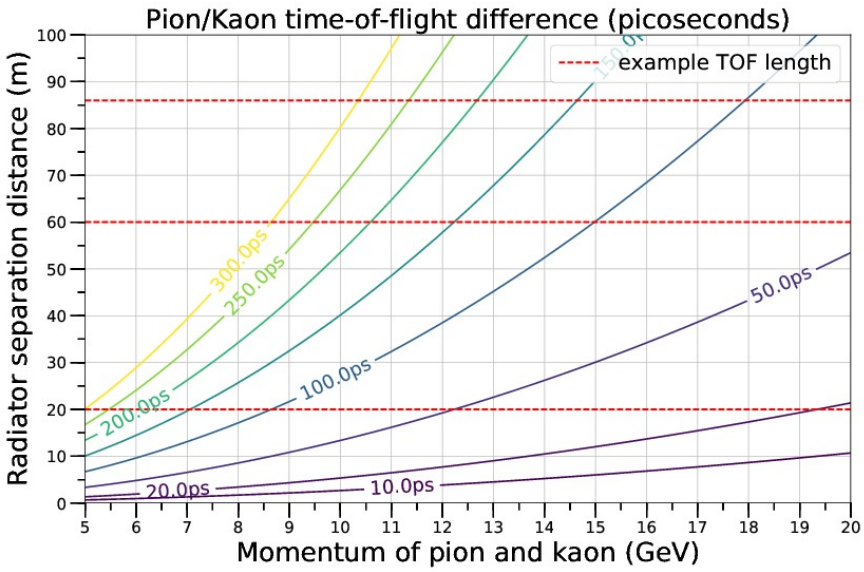

Figure 22: The contours of TOF difference between pions and kaons plotted versus particle momentum (abscissa) and the TOF detector separation (ordinate) with a scale that covers the 84m START/STOP separation of the current MINERVA TOF (Angelico).

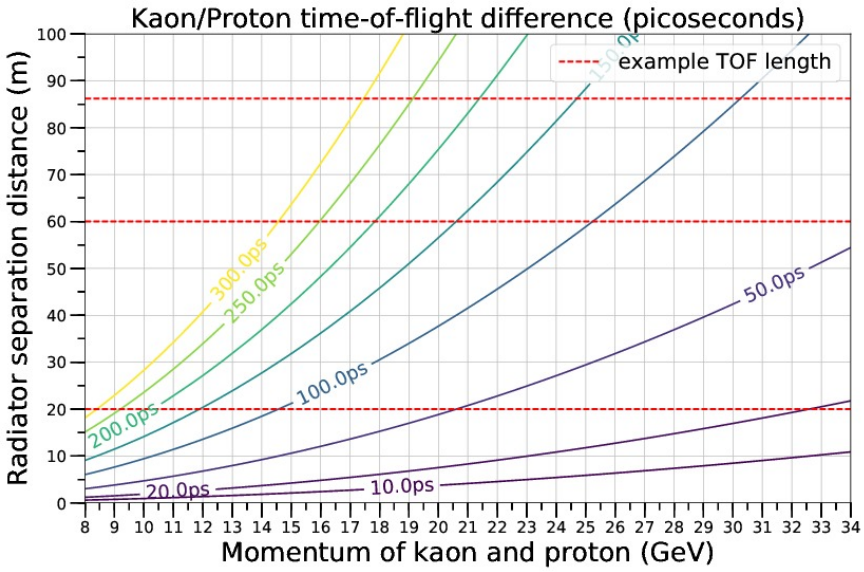

Figure 23: The contours of TOF difference between kaons and protons plotted versus particle momentum (abscissa) and the TOF detector separation (ordinate) with a scale that covers the 84m START/STOP separation of the current MINERVA TOF (Angelico).

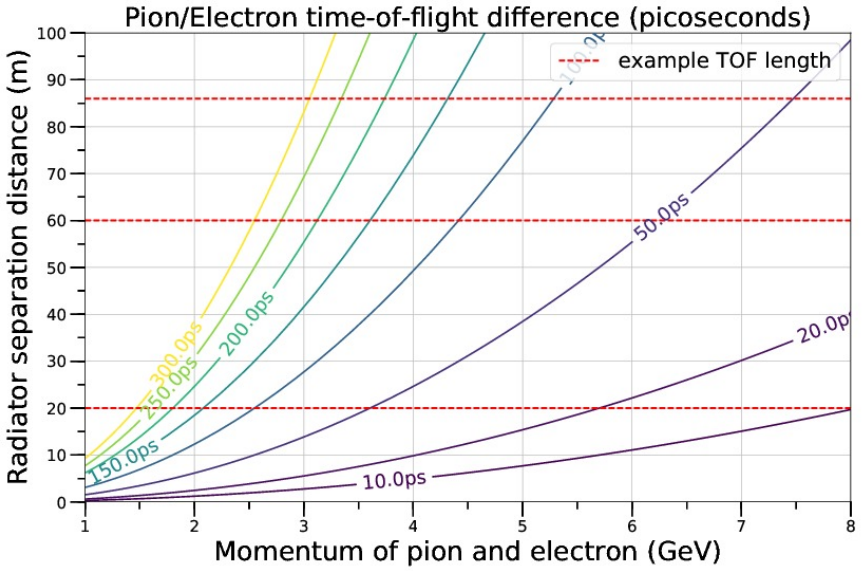

Figure 24: The contours of TOF difference between electrons and pions plotted versus particle momentum (abscissa) and the TOF detector separation (ordinate) with a scale that covers the 84m START/STOP separation of the current MINERVA TOF (Angelico).

Appendix B: 'Map' of the MTest Beam Line

Figures 25 and 26 give a 'map' of the MTest beam line.

		Beam Station	Beam Station
	INCHES	INCHES	Metres
MT3_GATEVALVE_750_CT	0.000	0.000	**0.000**
MT3CON_UP	103.253	103.253	**2.623**
MT3CON_DN	3.276	106.529	**2.706**
MT3SW_UP	19.329	125.858	**3.197**
MT3SW_DN	120.000	245.858	**6.245**
MT3BS_UP	19.374	265.232	**6.737**
MT3BS_DN	110.374	375.607	**9.540**
MT3Q3_UP	18.034	393.641	**9.998**
MT3Q3_DN	120.000	513.641	**13.046**
MT3Q4_UP	17.643	531.284	**13.495**
MT3Q4_DN	120.000	651.284	**16.543**
MT3W_UP	31.403	682.687	**17.340**
MT3W_DN	120.000	802.686	**20.388**
MT3U1-FLANGE_UP	18.557	821.243	**20.860**
MT3U1_UP	6.263	827.505	**21.019**
MT3U1_DN	120.009	947.514	**24.067**
MT3U1-FLANGE_DN	7.668	955.182	**24.262**
MT3U2_UP	256.858	1212.041	**30.786**
MT3U2_DN	120.198	1332.238	**33.839**
MT4TGT_UP	97.615	1429.854	**36.318**
MT4TGT_DN	12.000	1441.854	**36.623**
MTABS_UP	3.235	1445.090	**36.705**
MTABS_DN	73.273	1518.363	**38.566**
MT4Q1_UP	12.800	1531.163	**38.892**
MT4Q1_DN	120.000	1651.163	**41.940**
MT4W1_UP	13.247	1664.411	**42.276**
MT4W1_DN	120.001	1784.411	**45.324**
MTBABS-MT4Q2-BEAMPIPE	334.813	2119.225	**53.828**
MTBABS-MT4Q2-BEAMPIPE	64.059	2183.284	**55.456**
MT4Q2_UP	14.562	2197.846	**55.825**
MT4Q2_DN	120.000	2317.846	**58.873**
MT4W2_UP	24.970	2342.815	**59.508**
MT4W2_DN	120.000	2462.816	**62.556**
MT4Q3_UP	26.020	2488.835	**63.217**
MT4Q3_DN	120.000	2608.835	**66.265**
MT4VT_UP	102.253	2711.088	**68.862**
MT4VT_DN	30.000	2741.088	**69.624**
MT4FP_UP	145.318	2886.406	**73.315**
MT4FP_DN	7.644	2894.050	**73.509**
MT4CH1_UP	20.326	2914.376	**74.025**
MT4CH1_DN	67.500	2981.876	**75.740**
MT4HT_UP	321.912	3303.788	**83.916**
MT4HT_DN	29.999	3333.787	**84.678**
MT4Q4_UP	35.178	3368.966	**85.572**
MT4Q4_DN	120.000	3488.965	**88.620**

Figure 25: A list of the MTESTbeam elements and distances along the beamline- page 1 (courtesy of John Kyle)

MT4CH2_UP	14.769	3503.734	**88.995**
MT4CH2_DN	67.500	3571.234	**90.710**
MT4Q5_UP	49.925	3621.158	**91.978**
MT4Q5_DN	120.000	3741.158	**95.026**
MT4CV2_UP	13.428	3754.586	**95.367**
MT4CV2_DN	67.500	3822.086	**97.081**
MT4Q6_UP	64.826	3886.912	**98.728**
MT4Q6_DN	120.000	4006.912	**101.776**
MT5BEAMPIPE_UP	14.312	4021.224	**102.139**
MT5BEAMPIPE_DN	20.759	4041.983	**102.667**
MT4-TOF1_CT	32.974	4074.957	**103.504**
MT5SC_UP	7.534	4082.491	**103.695**
MT5CON_UP	12.905	4095.396	**104.023**
MT5VT1_UP	13.935	4109.331	**104.377**
MT5VT1_DN	29.999	4139.330	**105.139**
MT5E1_UP	18.753	4158.083	**105.616**
MT5E1_DN	120.000	4278.084	**108.664**
MT5E2_UP	19.357	4297.441	**109.155**
MT5E2_DN	120.056	4417.496	**112.205**
MT5E3_UP	18.402	4435.898	**112.672**
MT5E3_DN	120.000	4555.898	**115.720**
MT5E4_UP	19.508	4575.406	**116.216**
MT5E4_DN	120.000	4695.406	**119.264**
MT5E5_UP	19.051	4714.457	**119.747**
MT5E5_DN	120.000	4834.457	**122.795**
MT5Q1_UP	330.182	5164.640	**131.182**
MT5Q1_DN	120.000	5284.640	**134.230**
MT5Q2_UP	23.483	5308.122	**134.827**
MT5Q2_DN	120.000	5428.122	**137.875**
MT5VT2_UP	34.794	5462.916	**138.758**
MT5VT2_DN	30.001	5492.917	**139.520**
MT5HT2_UP	37.313	5530.230	**140.468**
MT5HT2_DN	29.412	5559.642	**141.215**
	5559.642		

Figure 26: A list of the MTESTbeam elements and distances along the beamline- page 2 (courtesy of John Kyle)

Appendix C: MIRCAT Time Resolution

While the MIRCAT geometry is not ideal for fast TOF measurements, it would allow us to get started on many of the aspects of the installation and commissioning of an LAPPD system at the FTBF. One question is whether or not it will be useful for characterization of the LAPPD time resolution as well as other, more accessible, parameters such as gain and uniformity. Figure 27 shows the time resolution derived from a simple TOF analysis assuming a TOF resolution of 0ps, 25ps, or 40ps, and a position resolution of 0.7 mm, on each photon arriving at the LAPPD[6].

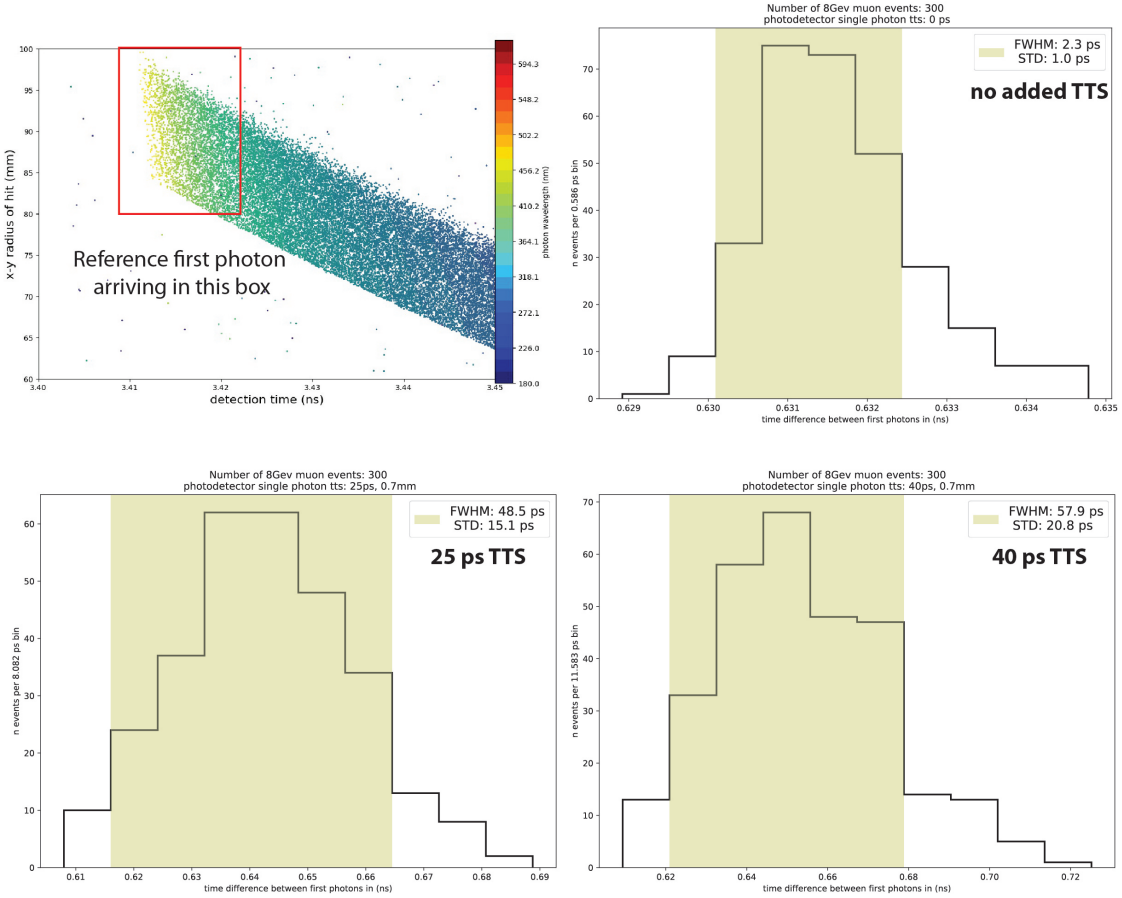

Figure 27: Upper left panel: Photons from the upstream radiator arrive at the LAPPD in a ring, with the earliest photons at a higher radius than later photons. The first photon that arrives within the high-radius red box is selected as a time reference. The distribution of photon time-of-flight is calculated by subtracting each photon arrival time from the time reference. The distribution is shown in the 3 histograms for detector single-photoelectron transit time Gaussian spreads (TTS) of 0ps, 25ps, and 40ps, respectively. In each case the efficiency for the photocathode, is assumed to be 33% peak at 300nm and 20% at 405nm, numbers achieved by Incom.

[6]We hasten to emphasize that the MIRCAT geometry is only a temporary solution to the problem of not having more than 1 LAPPD; once more LAPPDs are acquired the MIRCAT will be replaced with a higher-resolution conventional TOF geometry covering the entire beam profile using stations with a larger separation, and Cherenkov light produced only at the face of each photodetector.

References

[1] Incom Inc. Charlton Mass. See http://www.incomusa.com/

[2] Argonne National Laboratory, Fermi National Laboratory, Saclay/IRFU, Stanford Linear Accelerator Center, University of Chicago, University of Hawaii; Fermilab Experiment T979; H. Frisch, Spokesperson; Memorandum of Understanding, PSEC Collaboration; Fermilab, Batavia IL; Feb, 2008.

[3] J. Va'vra, D.W.G.S. Leith, B. Ratcliff, E. Ramberg, M. Albrow, A. Ronzhin, C. Ertley, T. Natoli, E. May, K. Byrum; *Beam Test of a Time-of-Flight Detector Prototype*; Nucl. Instr. Meth. A606, 404 (2009).

[4] A. Ronzhin et al., *Development of a 10 ps level time of flight system in the Fermilab Test beam facility*; Nucl. Instr. Meth. A623,931(2010).

[5] E. Oberla and H.J. Frisch; *Charged particle tracking in a water Cherenkov optical time-projection chamber*, Nucl. Inst. Meth. Phys. Res. A. Volume 814, 1 April 2016, Pages 19-32, ISSN 0168-9002; arXiv:1510.00947

[6] K. Inami, N. Kishimoto, Y. Enari, M. Nagamine, and T. Ohshima; *A 5-ps Tof-counter with an MCP-PMT*; Nucl. Instr. Meth. A560, p.303, 2006

[7] T. Credo, H. Frisch, H. Sanders, R. Schroll, and F. Tang; *Picosecond Time-of-Flight Measurement for Colliders Using Cherenkov Light* Proceedings of the IEEE, Rome, Italy, Oct. 2004; Nuclear Science Symposium Conference Record, 2004 IEEE, Vol. 1.

[8] B.W. Adams, A. Elagin, H. Frisch, R. Obaid, E. Oberla, A. Vostrikov, R. Wagner, J. Wang, M. Wetstein; *Timing Characteristics of Large Area Picosecond Photodetectors*; Nucl. Inst. Meth. Phys. Res. A. , Vol. 795, pp 1-11 (Sept. 2015);
Note that for high-gain detectors such as the LAPPD$^{\text{TM}}$, with signals consisting of multiple photons, such as from Cherenkov light, the determining factor is the length of time before the first photoelectron strikes the emissive surface. The photon statistics are consequently binomial and not Gaussian, providing a much faster improvement of time resolution than $1/\sqrt{N}$.

[9] M. Bogdan, H. J. Frisch, E. Oberla and M. Wetstein *A Modular Data Acquisition System using the 10 GS/s PSEC4 Waveform Recording Chip*; Paper for IEEE NSS/Mic RealTime 2016, Strasbourg, France Oct. 2016 ArXiV:1607.02395v1 8 Jul 2016

[10] John Podczerwinski; *Characterization of Self-Triggering on the PSEC4 Waveform Digitizing ASIC*; PSEC Document Library #329, lappdocs.uchicago.edu.

[11] B. Adams et al.; *A Brief Technical History of the Large-Area Picosecond Photodetector (LAPPD) Collaboration*; ArXiV:1603.01843

[12] See http://psec.uchicago.edu/library/

[13] See http://psec.uchicago.edu/library/doclib/

[14] See the talks by D. Breton, E. Delanges, and S. Ritt in *The Factors that Limit Time Resolution in Photodetectors*; Workshop, University of Chicago, Chicago, IL; 28-29 April 2011. See *h*ttp://psec.uchicago.edu/workshops/.

[15] H. J. Frisch; *Drifting Photons on Optical Paths, Mirrors, Sub-mm Resolution in Four Dimensions, and Transverse/Longitudinal Phase Space: Exploiting Psec Time Resolution*. To be published in the proceedings of the 5th International Conference on Micro-Pattern Gas Detectors (MPGD2017); 22-26 May, 2017, Philadelphia, USA; Proceedings in Science, 2018

[16] S. Ritt, in *The Factors that Limit Time Resolution in Photodetectors*; Workshop, Univ. of Chicago, Chicago, IL; 28-29 April 2011. See http://psec.uchicago.edu/workshops/ Note that of the values needed of the four parameters to achieve a time resolution of 100 fsec (the bottom row of the table of extrapolations), we have achieved or exceeded three: sampling rate, noise, and signal size. Only the analog bandwidth falls short at present.

[17] The University of Chicago has trademarked the LAPPD 203mm-square module to distinguish it from smaller MCP-PMT's, or fundamentally different designs. The trademarked name has been licensed to Incom Inc.

[18] H. J. Frisch; *Precision Measurements and Signature-Based Searches at the Tevatron*, XXXV International Meeting on Fundamental Physics, Santiago de Compostela, Spain; May, 2007. See http://hep.uchicago.edu/ frisch/#Talks

[19] S. Nagaitsev et al., *Quantum Effects in Undulators*; Proposal to the DOE, April 2018.

[20] See http://annie.uchicago.edu and
http://annie.uchicago.edu/lib/exe/fetch.php?media=pacmeeting_v2.1.pdf

[21] F. Tang, C. Ertley, J.-F. Genat, J. Anderson, K. Byrum, G. Drake, E. May, and G. Sellberg *Transmission-Line Readout with Good Time and Space Resolutions for Planacon MCP-PMTs*, in Topical Workshop on Electronics for Particle Physics, CERN, pp. 579-583, 2008

[22] E. Oberla, J.-F. Genat, H. Grabas, H. Frisch, K. Nishimura, and G. Varner; *A 15 GSa/s, 1.5 GHz Bandwidth Waveform Digitizing ASIC*, Nucl. Instr. Meth. A735, 21 Jan., 2014, 452;

[23] E. Oberla, J. Porter, and J. Stahoviak; *PSEC4A : A 10 GSa/s Waveform Sampling ASIC with Multi-Event Buffering Capability*; Proceedings of TWEPP 2018; Antwerp, Belgium (Sept. 2018)
indico.cern.ch/event/697988/.../2776726/TWEPP_Porter_poster_163.pdf;

[24] The group at Photek has built an exceptionally fast small MCP-based PMT with a 60-psec risetime; J. Milnes and J. Howorth, Photek Ltd; Proc. SPIE vol 5580 (2005) pp 730-740.

[25] Photonis, Planacon^{TM}; see the Planacon link at
http://www.photonis.com/en/product/. We thank Greg Sellberg for his development of the technique to connect the 1024 anode pads to the strips.

[26] I. Adam, R. Aleksan, L. Amerman, E. Antokhin, D. Aston et al..
The DIRC Particle Identification System for the BABAR Experiment;
Nucl. Inst. and Meth. **A**538, 281 (2005)

[27] M. Rominsky, Hadron Production Workshop, July 2017;
https://indico.fnal.gov/event/14938

[28] M. Backfish, L. Bellantoni, A. Norrick, A. Ronzhin, G. Savage; *Time Of Flight for MTest* Fermilab Tech Note Version 6/14/18; available at http://psec.uchicago.edu/library/TOF_Systems/

[29] Leo Bellantoni; private communication.

[30] See, for example, http://www.ti.com/clock-and-timing/jitter-cleaners/products.html

[31] *Meson Test Beam Cherenkov Counter Gas and Vacuum System Documentation*; 3/5/07;
http://psec.uchicago.edu/library/Cherenkov_Counters_MTest

[32] E. Angelico, T. Seiss, B.W. Adams, A. Elagin, H. Frisch, E. Oberla, E. Spieglan; *Capacitively coupled Pulse Readout in a 20cm×20cm MCP-based photodetector* Nucl. Instr. Meth. A, 2016

[33] J. W. Elam, A. U. Mane, J. A. Libera, J. N. Hryn, O. H. W. Siegmund, Jason McPhate, M. J. Wetstein, A. Elagin, M. J. Minot, A. O'Mahony, R. G. Wagner, W. M. Tong, A. D. Brodie, M. A. McCord, and C. F. Bevis;
Synthesis, Characterization, and Application of Tunable Resistance Coatings Prepared by Atomic Layer Deposition; ECS Transactions, 58 (10) 249-261 (2013)

[34] A. Lehmann et al *Lifetime of MCP-PMTs and other performance features*; JINST 13, C02010 (2018). We note that the improved performance is due to the development of ALD coatings by N. Sullivan and J. Elam, specifically for this purpose.

[35] JJ Schmidt, private communication.

[36] We thank John Kyle of the Fermilab Alignment and Metrology Department for these documents.

[37] Mesut Caliskan, *Real-Time Remote Control of Droege HV Power Supplies*;
http://lappddocs.uchicago.edu/